Supplementary Information

All-textile, chip-less, battery-free body sensor networks enabled by a concentric multi-node hub antenna architecture

Juneyeong Lee[1], Mugeun Lee[1], Jinho Kim[1], Hwajoong Kim[1], Jongbin Yu[2], Namjung Kim[2], and Jaehong Lee[1*]

[1] Department of Robotics and Mechatronics Engineering, DGIST, Daegu 42988, Republic of Korea

[2] Department of mechanical engineering, Gachon Unviersity (GCU), Gyeonggi-do, Republic of Korea

*Corresponding author. E-mail: jaelee@dgist.ac.kr

Keywords: body sensor network, textile electronics, fiber electronics, wearable sensing platform, smart textiles

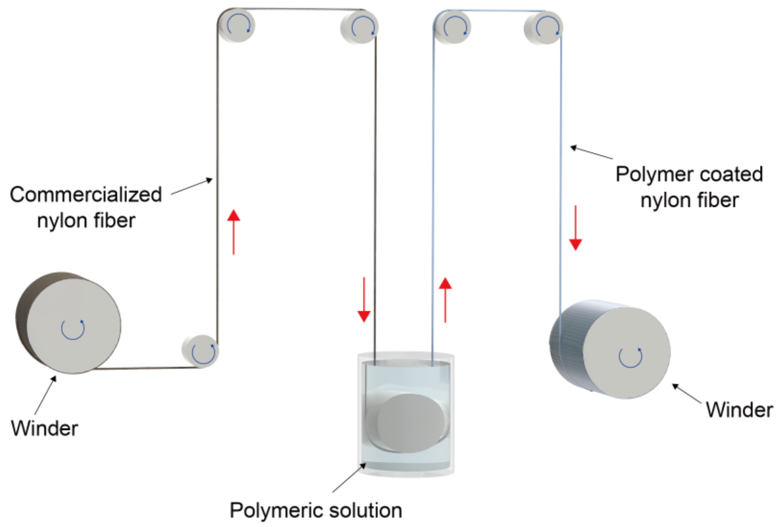

Supplementary Figure 1. Schematic illustration of the dip-coating process for polymeric layer on the surface of nylon fiber scaffold.

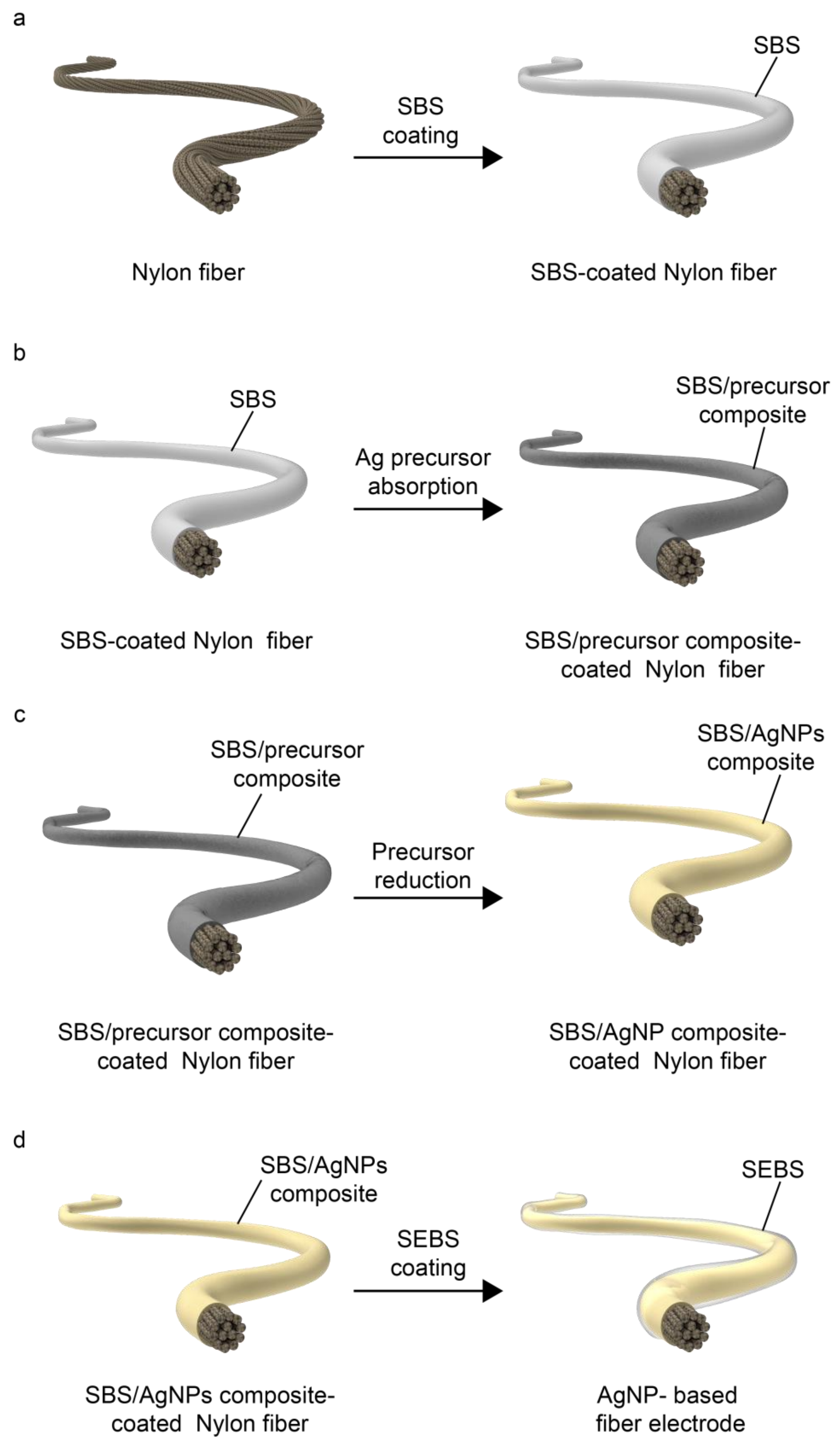

Supplementary Figure 2. Fabrication process of the AgNPs-based flexible fiber electrode. **a** A nylon fiber is uniformly coated with an SBS layer using a dip-coating process. **b** The SBS-coated nylon fiber is fully immersed in an ethanol-based solution containing Ag precursors for

30 minutes, allowing Ag ions to be absorbed into the SBS layer, followed by air drying for 20 minutes. **c** The SBS/precursor composite-coated nylon fiber is then immersed in an ascorbic acid solution in DI water and placed in a 60°C oven for 1 hour to directly reduce the absorbed Ag ions into AgNPs. The absorption and reduction processes of Ag ions in the SBS-coated fiber are repeated to increase the AgNPs content in the fiber electrode. **d** The SBS/AgNPs composite-coated nylon fiber is then coated with a uniform SEBS layer using a dip-coating process to prevent electrical shorting.

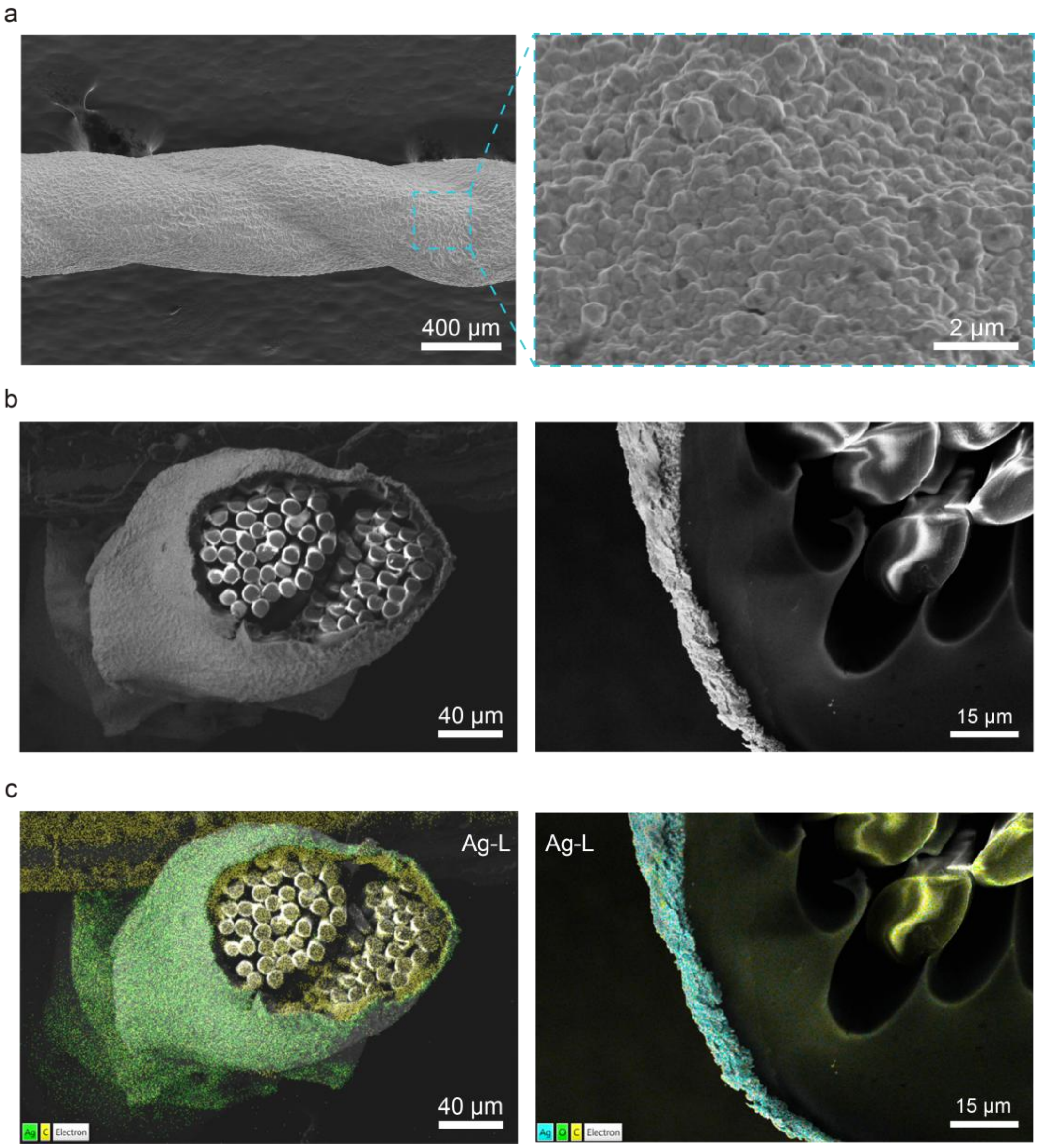

Supplementary Figure 3. a The SEM image of the surface of the AgNP-based flexible fiber electrodes, **b** The Cross-sectional SEM image of the AgNP-based flexible fiber electrodes and **c** the corresponding EDS mapping image of the AgNP-based flexible fiber electrodes.

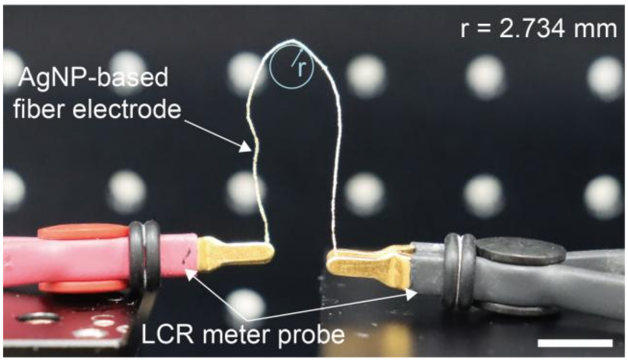

Supplementary Figure 4. Photograph showing the AgNPs-based flexible fiber electrodes subjected to a bending radius of 2.73mm. Scale bar: 1 cm.

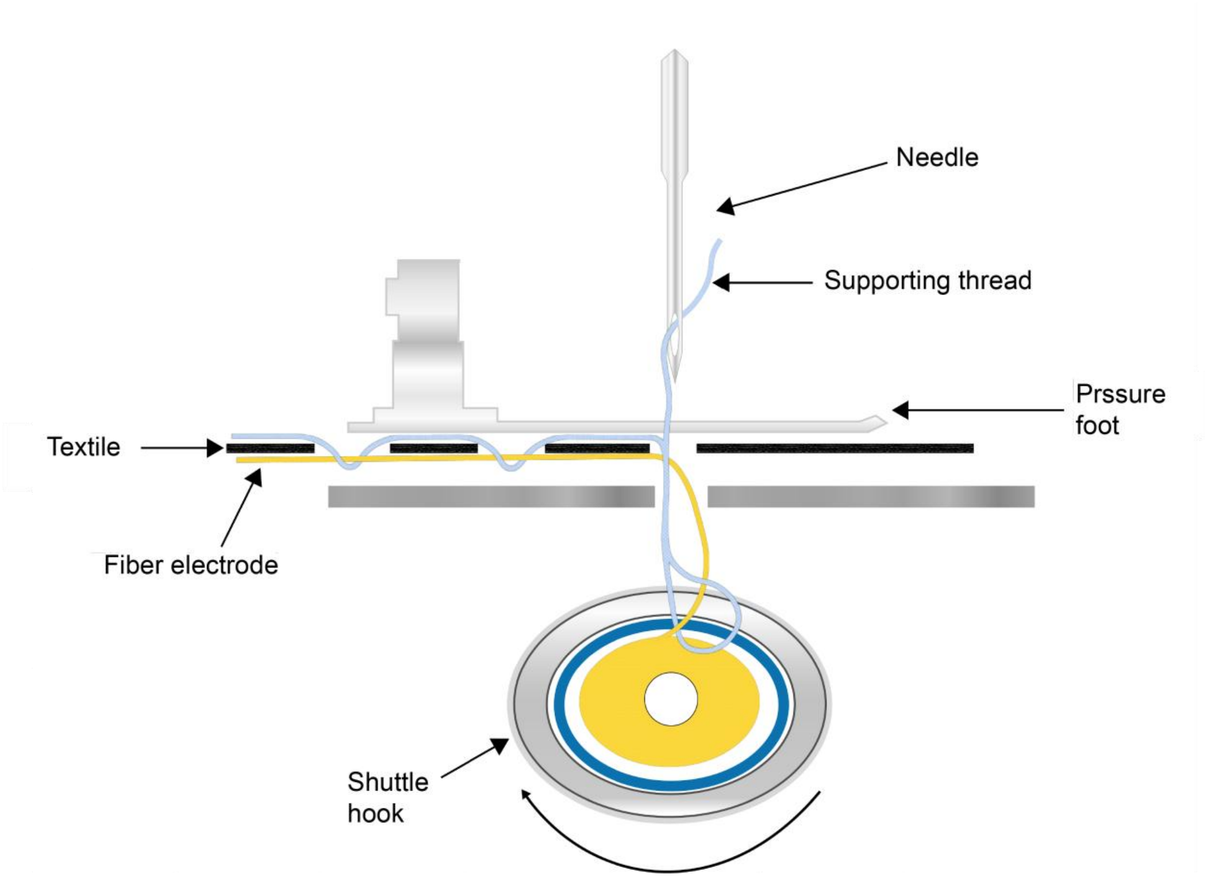

Supplementary Figure 5. Schematic illustration of the working mechanism of the digital embroidery machine.

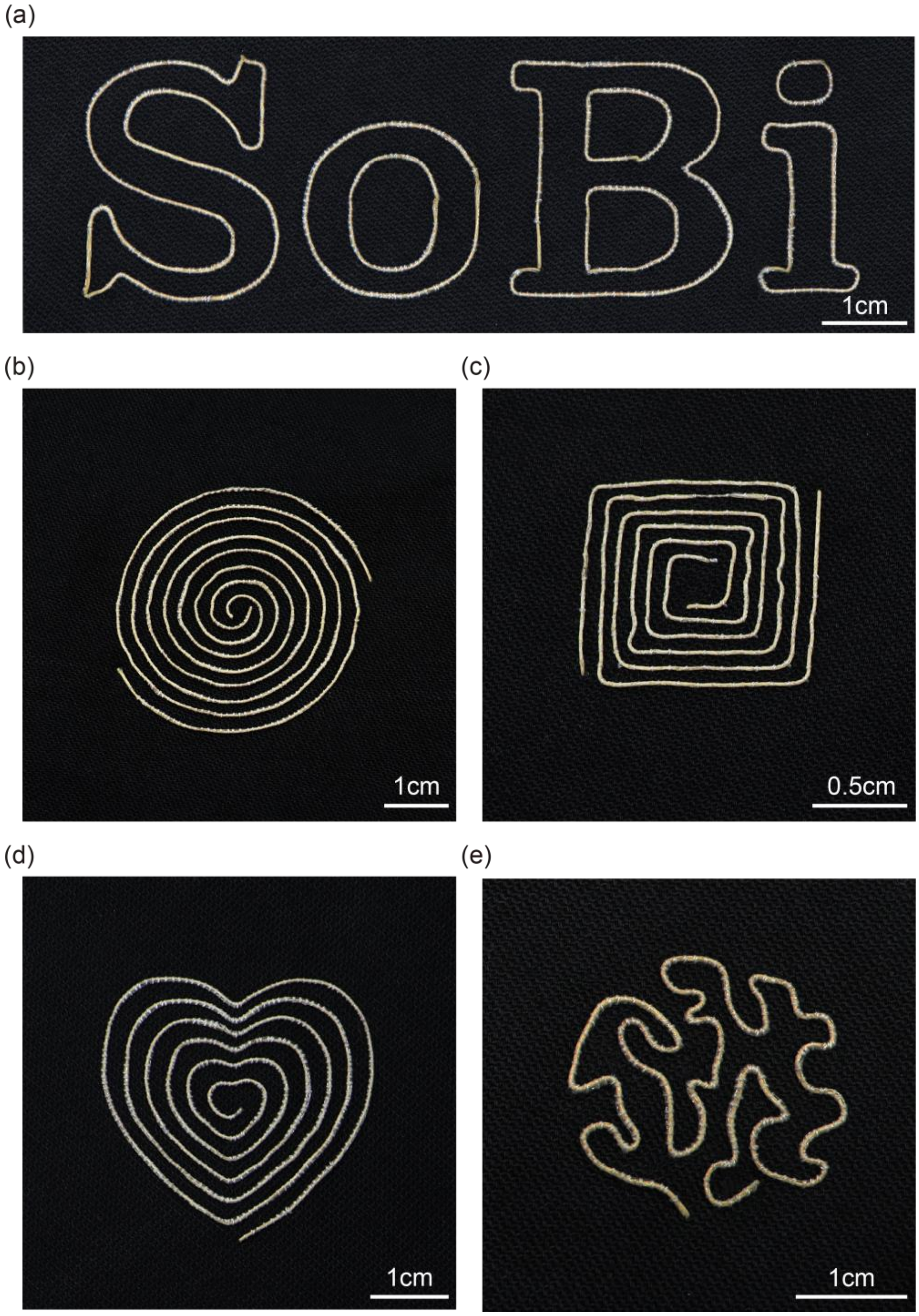

Supplementary Figure 6. Photographs showing various designs of patterned AgNP-based flexible fiber electrodes. **a** text pattern "SoBi", **b** circular double spiral pattern, **c** rectangular double spiral pattern **d** heart-shaped spiral pattern **e** Random-shaped pattern.

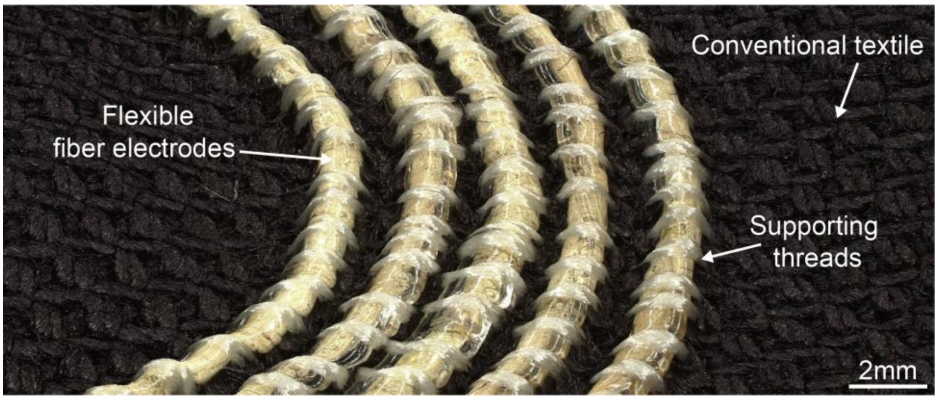

Supplementary Figure 7. Magnified image of the hub antenna in the textile-based sensor network.

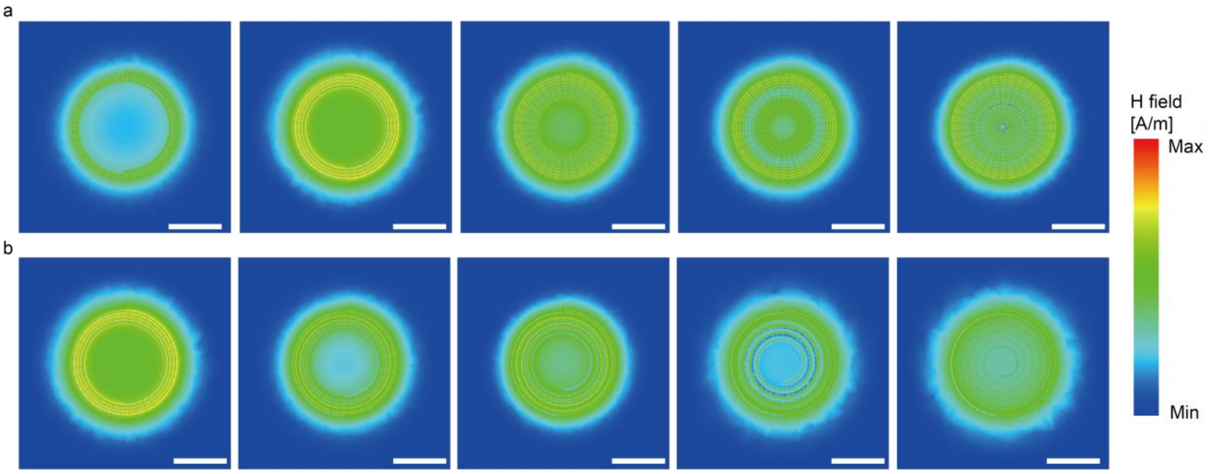

Supplementary Figure 8. a Simulated magnetic-field distributions for antenna coils with varying number of turns (from left: 3turns, 5turns, 10turns, 15turns, 20turns) and **b** varying fill factors (from left: 0.194, 0.269, 0.345, 0.456, 0.569). Scale bar:2 cm.

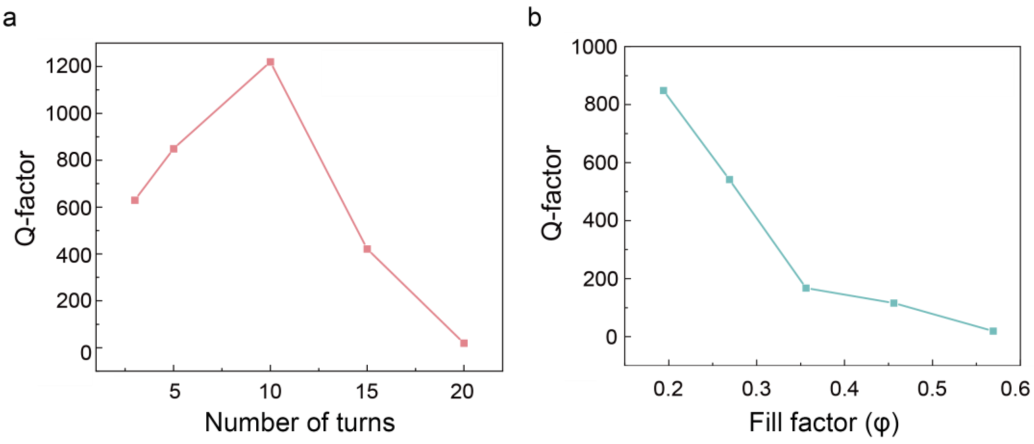

Supplementary Figure 9. a Measured Q-factor according to increasing number of turns and **b** varying fill factor of the antenna coil.

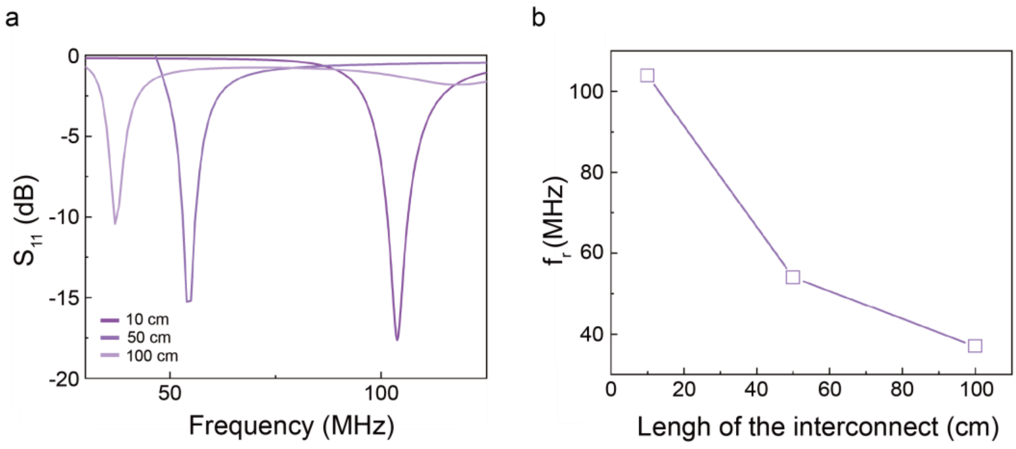

Supplementary Figure 10. a Simulated reflection coefficient spectra and **b** the corresponding resonant frequency of the single-node textile-based sensor network with varying length of the interconnects.

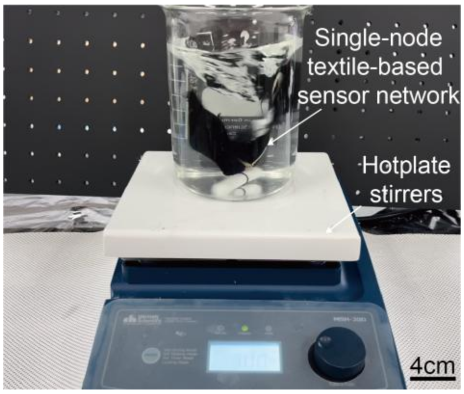

Supplementary Figure 11. Photograph showing the experimental setup for washing stability test of the textile-based sensor network. The washing protocol included sequential stirring steps of 30 minutes in 40°C DI water, 30 minutes in 40°C DI water with detergent, followed by drying step in a forced convection oven for 50°C for 30 minutes.

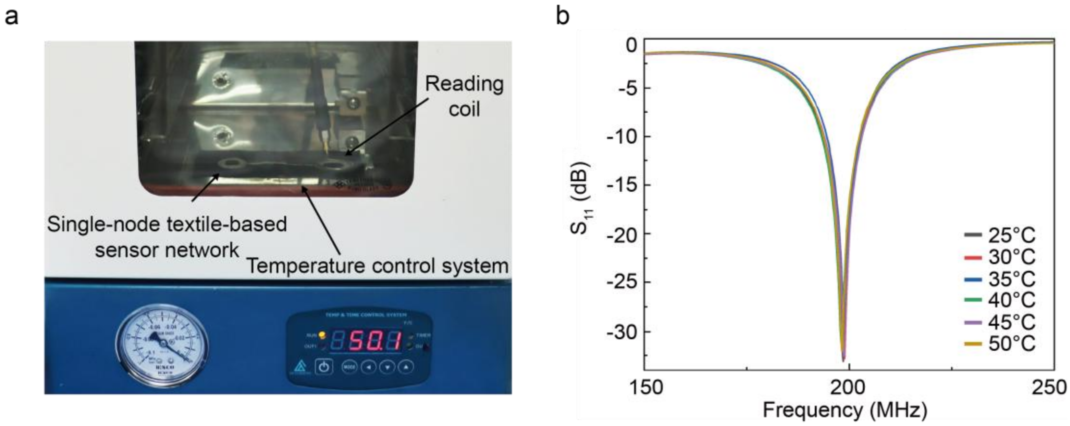

Supplementary Figure 12. a Photograph showing the experimental setup for stability test of the textile-based sensor network under temperature changes. **b** Reflection coefficient spectra of single-node textile-based sensor network under temperature changes. The sensor network exhibited excellent stability against the change in environmental temperature.

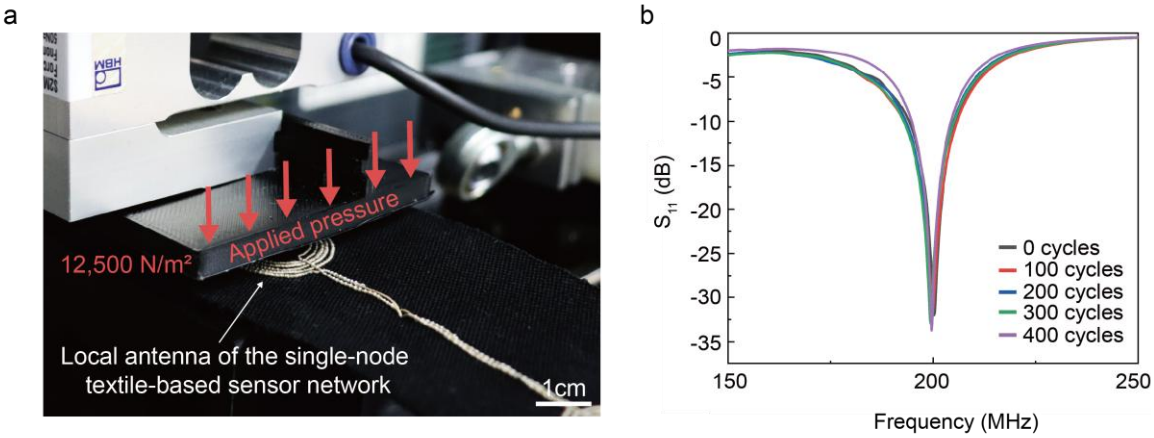

Supplementary Figure 13. a Photograph showing the experimental setup for stability test of the textile-based sensor network under cyclic pressure of 12.5 kPa. Scale bar: 1 cm. **b** Reflection coefficient spectra of single-node textile-based sensor network according to the cyclic pressure. The sensor network stably maintained the resonant properties under the external pressure.

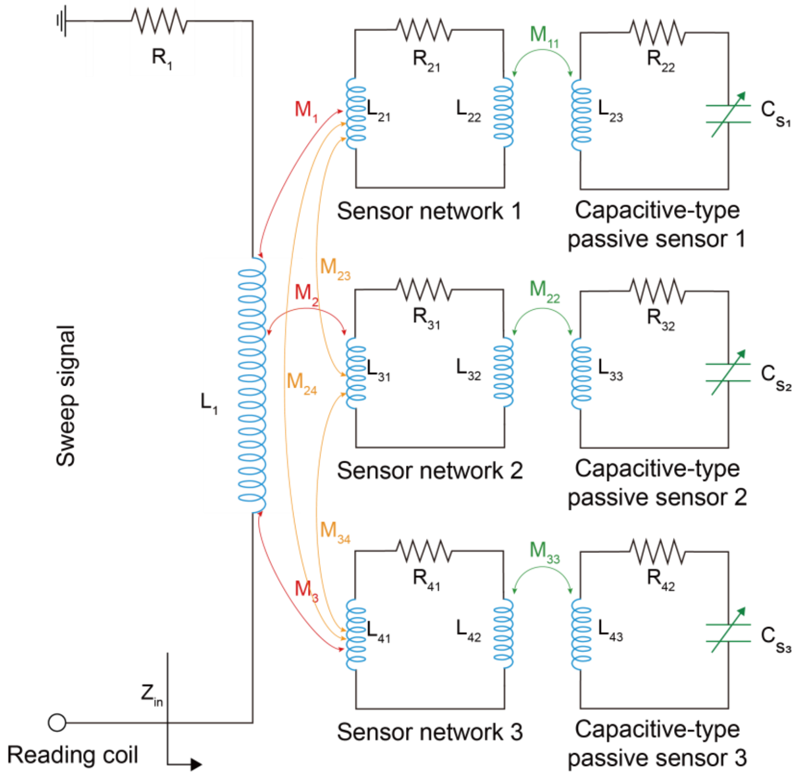

Supplementary Figure 14. Circuit diagram of the tBSN coupled with external reading coil and three passive body sensor systems.

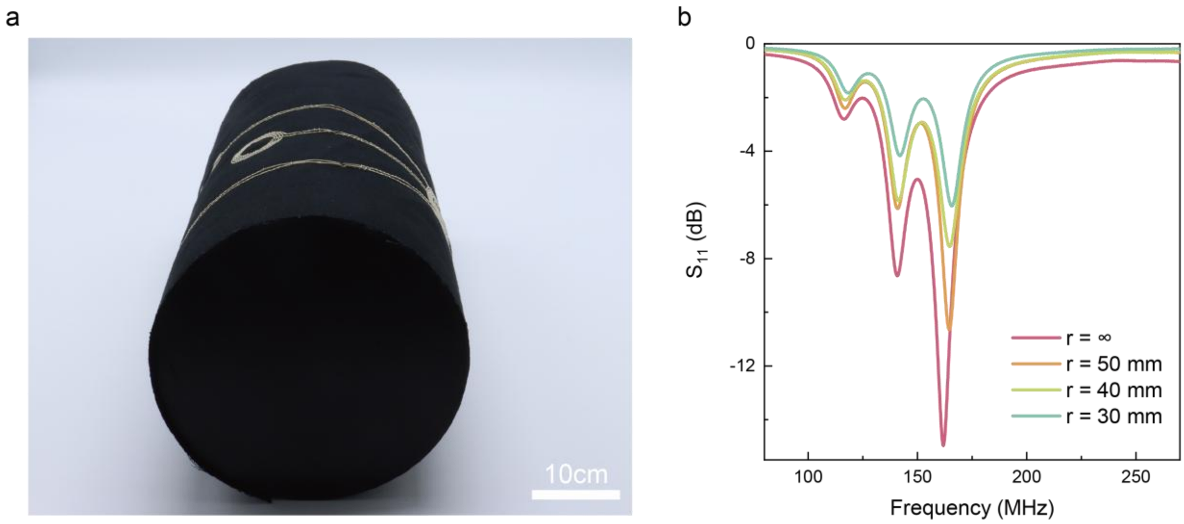

Supplementary Figure 15. a Photograph of the tBSN under bending deformation applied to the entire structure. **b** Reflection coefficient spectra of the tBSN measured under various bending radii.

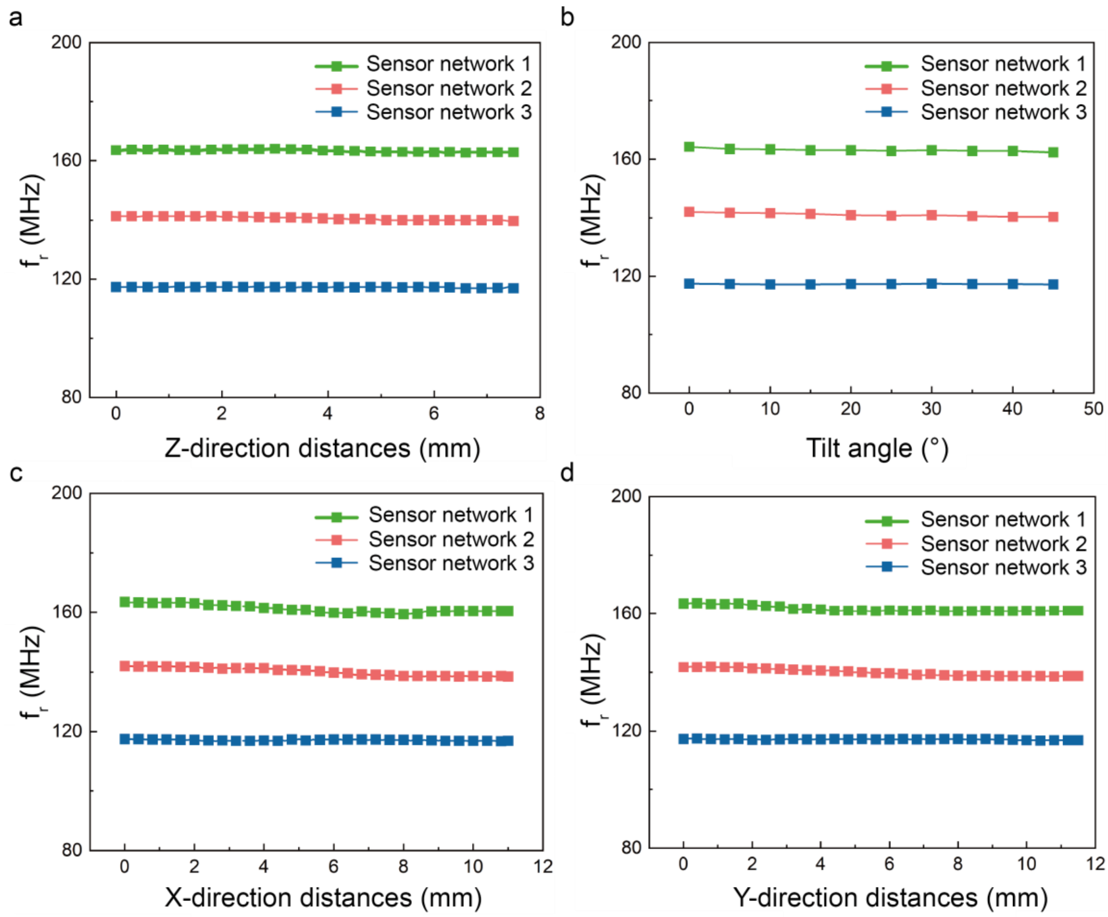

Supplementary Figure 16. Change in the resonant frequency of the tBSN under **a** various vertical separation distances, **b** different tilt angles, **c** x-directional misalignment, and **d** y-directional misalignment between the central hub antenna and the external reading coil.

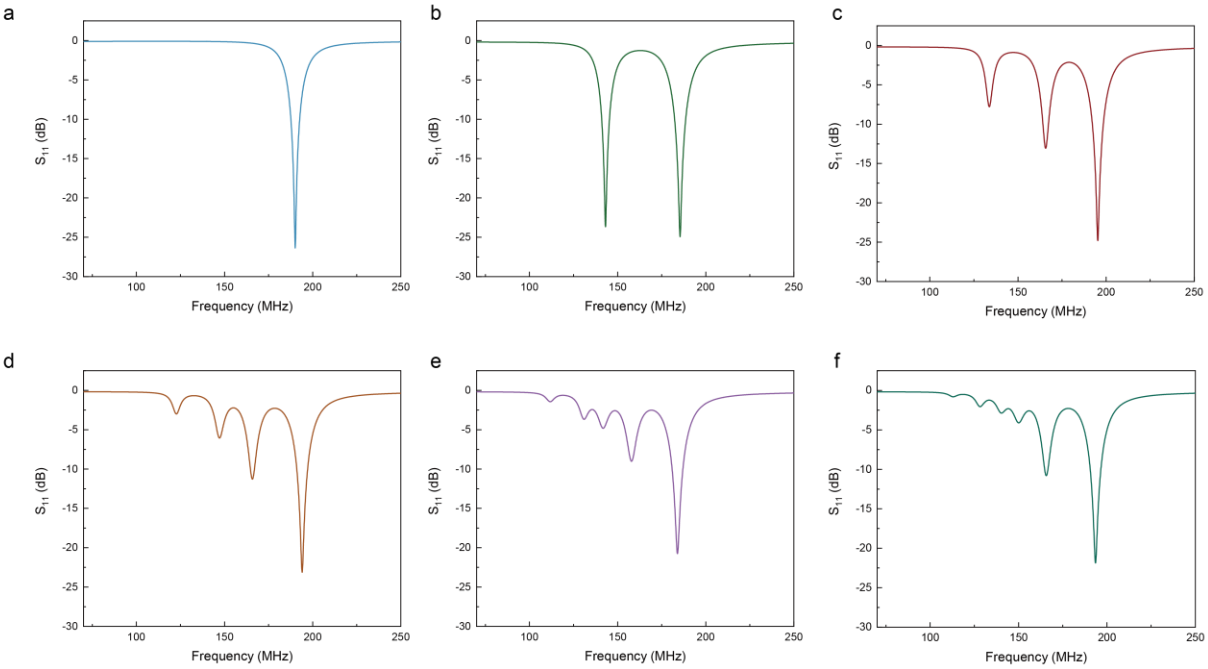

Supplementary Figure 17. a-f) Simulated Reflection coefficient (S11) spectra of tBSN with varying numbers of single-node sensor network in the system (from single to six nodes).

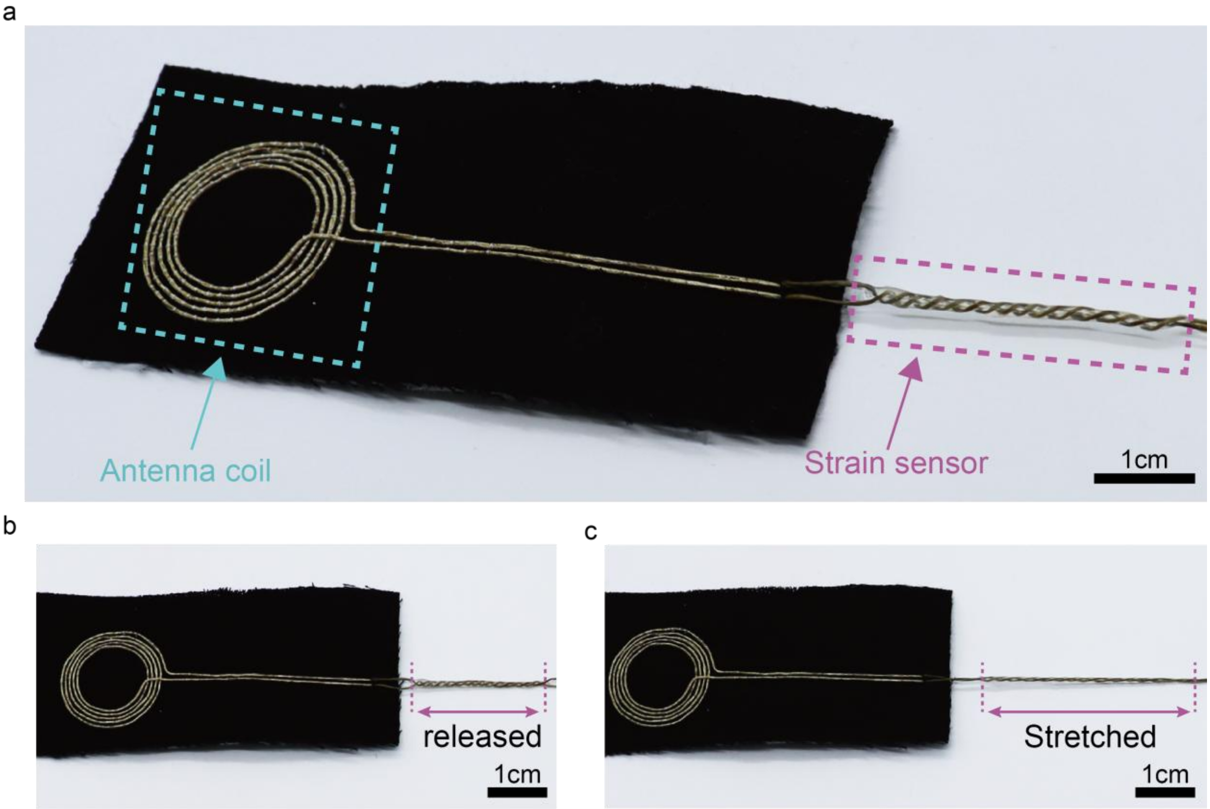

Supplementary Figure 18. a Photograph showing the wireless, and chip-less capacitive strain sensing system. **(b-c)** Photographs of the sensor in (b) a released state and (c) a stretched state. Scale bar: 1cm. Under external strain, the capacitance of the fiber strain sensor increases, which thereby deceases the resonant frequency of the sensing system.[1]

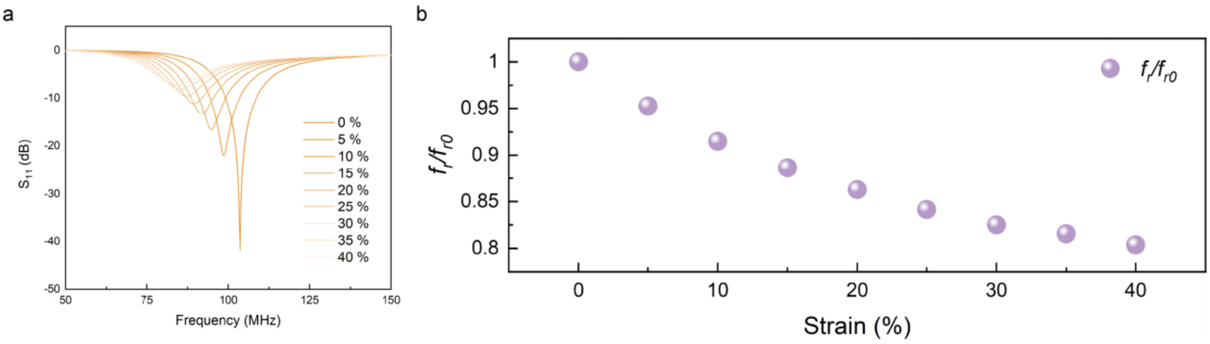

Supplementary Figure 19. a Reflection coefficient spectra of the wireless and chip-less capacitive strain sensing system under different strains applied to the fiber strain sensor, ranging from 0% to 40%. **b** Normalized resonant frequency of the strain sensing system under the different applied strains ranging from 0% to 40%.

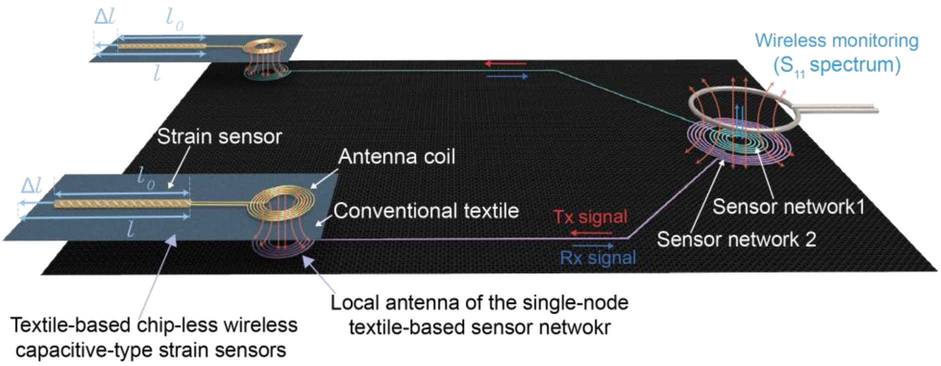

Supplementary Figure 20. Schematic illustration showing the simultaneous monitoring of multiple passive body sensors within a single scan using the tBSN.

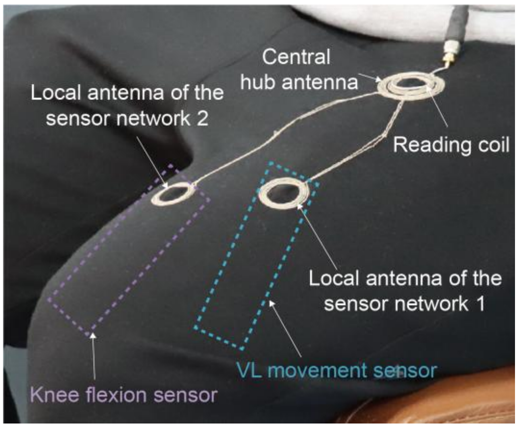

Supplementary Figure 21. Magnified image of the subject wearing the tBSN garment coupled with two passive sensors. Each passive sensor was precisely affixed inside the tBSN garment by sewing, such that the antenna coil of the passive sensor was aligned with the corresponding local antenna in the sensor network.

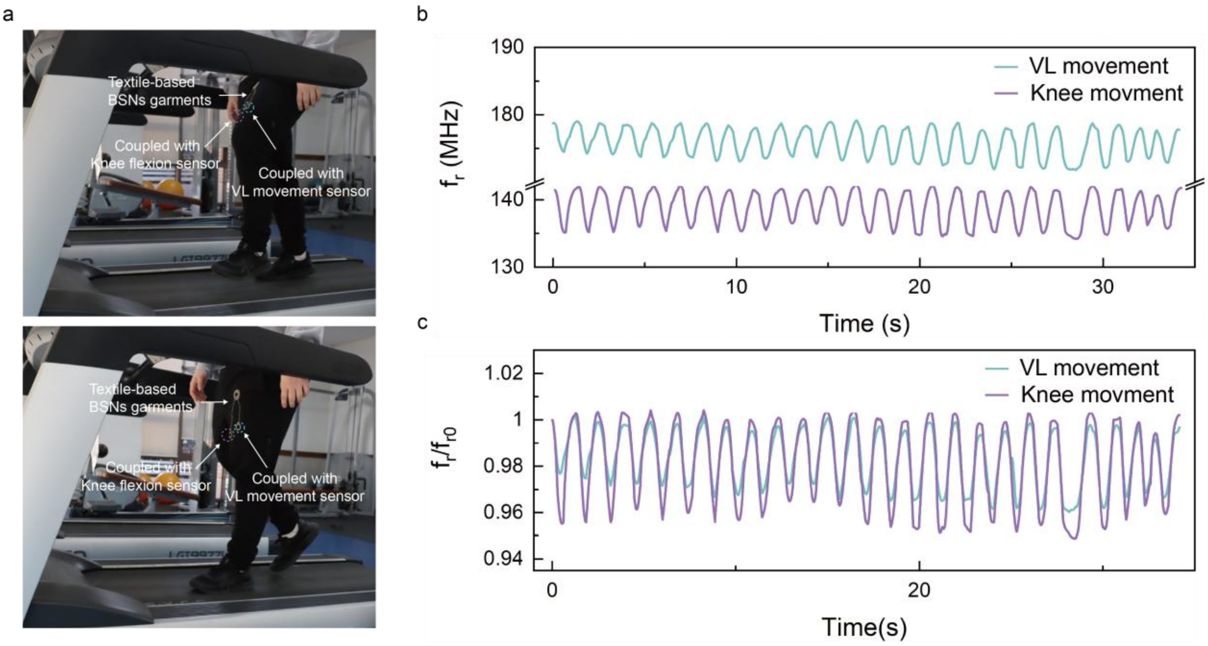

Supplementary Figure 22. Schematic illustration showing the simultaneous monitoring of multiple passive body sensors within a single scan using the tBSN.

Supplementary notes

Analytical modeling of the coupled circuit between a single-node textile-based sensor network and a chip-less passive sensor

Supplementary Figure 22 a presents a schematic illustration of the single-node textile-based sensor network, where the reading coil and chip-less passive sensor are inductively coupled. To model the network's response based on the behavior of the chip-less passive sensor, Kirchhoff's voltage law is applied to the equivalent circuit, as shown in Supplementary Figure 22 b.

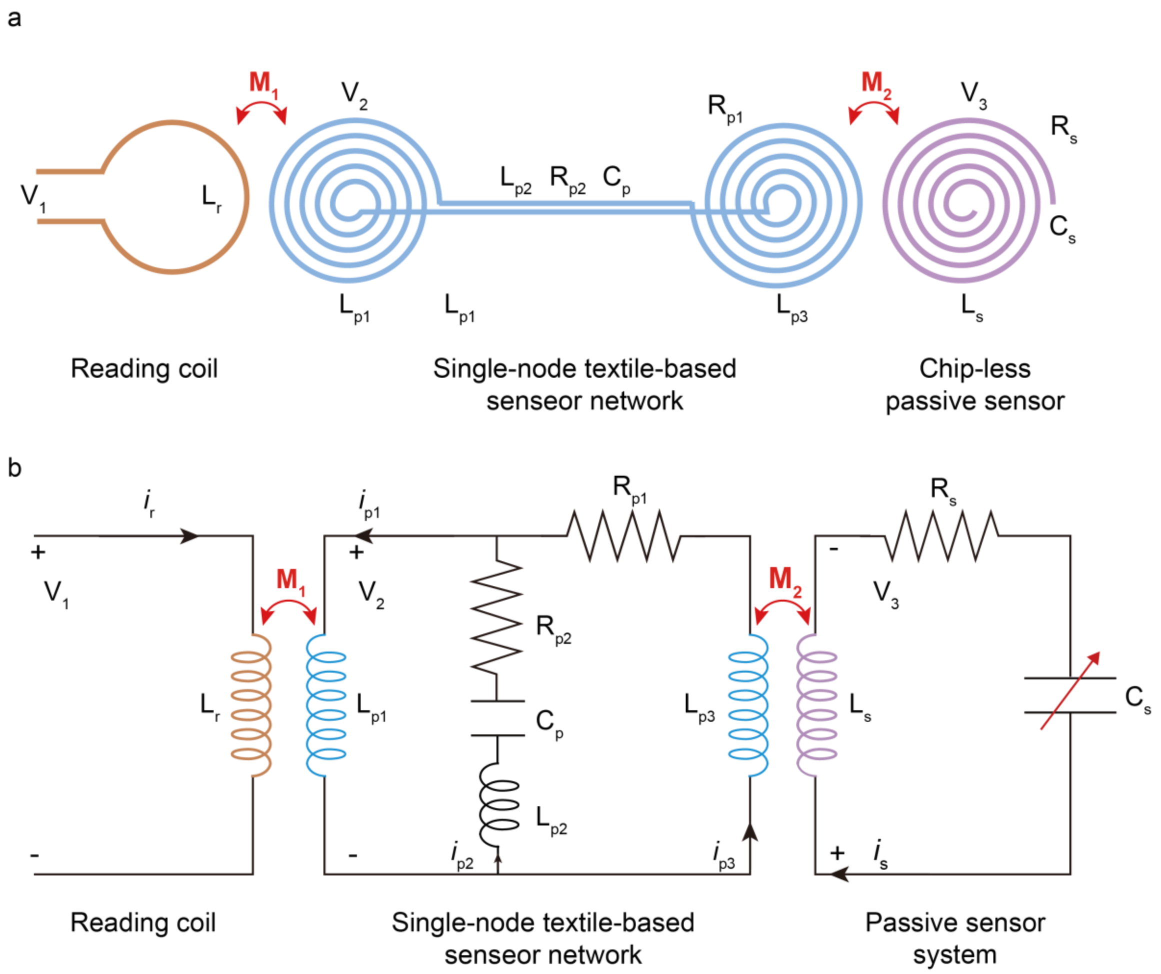

Supplementary Figure 23. a Schematic illustration of the inductive coupling between the chip-less passive sensor and the reading coil in a single-node textile-based sensor network. **b** Equivalent circuit model representing the inductive coupling between the chip-less passive sensor and the reading coil in the single-node textile-based sensor network.

The vector network analyzer (VNA) performs a frequency sweep by applying sinusoidal signals to the reading coil, which is inductively coupled to the single-node textile-based sensor network. The resulting voltages at the nodes defined in Supplementary Figure. 22 b. can then be expressed as follows[2].

$$V_1 = j\omega L_r i_r + j\omega M_1 i_{p1} \tag{1}$$

$$\begin{aligned} V_2 = j\omega L_{p1} i_{p1} + j\omega M_1 i_r &= -j\omega L_{p2} i_{p2} - \frac{i_{p2}}{j\omega C_p} - R_{p2} i_{p2} \\ &= -j\omega L_{p3} i_{p3} + R_{p1} i_{p3} - j\omega M_2 i_s \end{aligned} \tag{2}$$

$$V_3 = j\omega L_s i_s + j\omega M_2 i_{p3} = -R_s i_s - \frac{i_s}{j\omega C_s} \tag{3}$$

Where L_r denotes the inductance of the reading coil, and $L_s, C_s,$ and R_s represent the inductance, capacitance and resistance of the chip-less passive sensor. The mutual inductances M_1, M_2 are expressed as follows:

$$M_1 = k_1 \sqrt{L_r L_{p1}} \tag{4}$$

$$M_1 = k_1 \sqrt{L_r L_{p1}} \tag{5}$$

Here, L_{p2} denotes the inductance of the interconnect between the hub and the local antenna within the single-node textile-based sensor network, while C_P represents the equivalent capacitance of the single-node textile-based sensor network. The resulting impedance observed at the terminals of the reading coil can be described as follows:

$$Z = \frac{V_1}{i_r} = j\omega L_r + \frac{\omega^2 {M_1}^2}{j\omega L_{p1} - \frac{\alpha\beta}{\alpha + \beta}} \tag{6}$$

$$where\ \alpha = -j\omega L_{p2} - \frac{1}{j\omega C_p} - R_{p2}, \beta = -j\omega L_{p3} - R_{p1} + Z_s \quad (7)$$

$$Z_s = \frac{\omega^2 {M_2}^2}{R_s + j\omega L_s + \frac{1}{j\omega C_s}} \quad (8)$$

Here, Z_s represent the impedance of the chip-less passive sensor. The magnitude of the $|S_{11}|$ calculated from Eq. (S6) exhibits two distinct resonance peaks, which originate from the chip-less passive sensor and single-node textile-based sensor network, respectively. According to Eq. (S8), the chip-less passive sensor resonates at specific frequency given by $\omega_s = \frac{1}{\sqrt{L_s C_s}}$, while single-node textile-based sensor network exhibits resonance when the $j\omega L_{p1} - \frac{\alpha\beta}{\alpha+\beta} = 0$ is holds. Since the single-node textile-based sensor network and the chip-less passive sensor are inductively coupled through mutual inductance M_2, variations in ω_s due to changes in C_s (caused by external stimuli) influence the resonance condition of the single-node textile-based sensor network. As indicated in Eq. (S8), variations in C_s directly affect the sensor impedance Z_s, which alters β, and modifies the resonance condition $j\omega L_{p1} - \frac{\alpha\beta}{\alpha+\beta} = 0$ of the textile-based single-node sensor network. This interaction consequently leads to a shift in the resonance frequency of the single-node textile-based sensor network.

Reference

1 Lee, J. *et al.* Stretchable and suturable fibre sensors for wireless monitoring of connective tissue strain. *Nature Electronics* **4**, 291-301 (2021).

2 Chan, Y. J. *et al.* Positionally-independent and extended read range resonant sensors applied to deep soil moisture monitoring. *Sensors and Actuators A: Physical* **333**, 113227 (2022).